condensed matter

MDPI

Article

Two-Band Electronic Reconstruction Induced via Correlation and CDW Order Effects

L. Craco

Institute of Physics, Federal University of Mato Grosso, Cuiabá 78060-900, MT, Brazil; lcraco@fisica.ufmt.br

Abstract: The emergence of a charge density wave (CDW) in transition-metal dichalcogenides opens up a route to charge order, followed by superconductivity at low temperatures. A key question here concerns how many particle electron–electron interations govern the low-energy electronic structure in the normal and CDW states. Using dynamical mean-field theory, we explore the many-body properties of an extended, two-band Hubbard model applicable to $2H$-$TaSe_2$. We reveal the electronic structure reconstruction in the normal and CDW states driven by two-band dynamical correlations. Our results demonstrate a remarkable renormalization of the Ta-5*d* bands crossing the Fermi level, showing a continuous reduction in the CDW gap up to an incomplete gapping, followed by a CDW to a CDW–Mott phase transition pertinent to strongly correlated transition-metal dichalcogenides.

Keywords: Hubbard model; two-band; CDW; density of states

Citation: Craco, L. Two-Band Electronic Reconstruction Induced via Correlation and CDW Order Effects. *Condens. Matter* **2024**, *9*, 42. https://doi.org/10.3390/condmat9040042

Academic Editor: Krzysztof Wohlfeld

Received: 16 September 2024
Revised: 25 October 2024
Accepted: 28 October 2024
Published: 30 October 2024

1. Introduction

The relationship between the dimensionality of a lattice and the correlation between electrons is a long-standing issue in the fields of condensed matter and material physics, particularly in regard to the emergence of diverse quantum phases. A correlated electron system is defined by the presence of significant to pronounced many-particle Coulomb interactions between electrons, which give rise to a distinct set of physical properties that are not observed in a weakly interacting electron system. The most significant consequence of electron correlation is the Mott metal–insulator transition [1–3], which occurs when a half-filled paramagnetic metal is converted into a correlated insulator when the on-site Coulomb interaction, U, exceeds the bare bandwidth, W (i.e., the effective Coulomb interaction to bandwidth U/W ratio). Consequently, following decades of fundamental and applied research, it has been established that the impact of electron–electron interactions in correlated electron systems is contingent upon the ratio of energy scales between U and W. In the limit of small U/W, the electronic properties are predominantly governed by electron hopping and electron–phonon interactions [4]. Conversely, when $U/W \approx 1$, electron–electron interactions become a dominant factor, and in the limit of large U/W, the double occupancy of electrons on a single site is prohibited [5]. This results in a Mott insulating state at half-filling [1–3], which could lead to the emergence of novel electronic states such as superconductivity (unconventional or not) upon external perturbations [6–13]. Interesting examples in this context are the transition-metal dichalcogenides $(1T, 2H)$-MX_2 (M = Ta X = S,Se), which are considered to be systems with similar U and W energy scales [14–17]. As common to this material class, charge density wave (CDW)-phase instabilities [17–21] coexisting with superconductivity [21–23] emerge at low temperatures (T). Interestingly, while the low-T commensurate CDW phase of $1T$-TaS_2 is considered to be a Mott insulator [24,25] because of the half-filling insulating behavior [12,26–29], the monolayer $1T$-$TaSe_2$ shows a CDW–Mott phase transition around 530 K [17], which has also been reported for heterogeneous Ta-dichalcogenide bilayers [30]. Also noteworthy is that both the commensurate and incommensurate CDW phases lead to incomplete gapping or pseudogapped electronic excitations at low energies [21,22,31–33] similar to that observed in high-T_C cuprates [34–37]

due to their proximity to Mottness [38]. Motivated thereby, here, we show the emergence of a pseudogap regime as the precursor to the CDW–Mott phase [17] in a two-band ($\mathcal{TB}$) model relevant to 2H-$TaSe_2$ [39].

In recent decades, transition-metal dichalcogenides have been the subject of extensive study due to the intrinsic electronic properties resulting from the interplay between the lattice structure, CDW ordering, disorder, and electron–phonon and electron–electron correlation effects. These effects have been the subject of numerous studies, as evidenced by the extensive literature on the topic [17,20,21,24,25,28,29,31,39–48]. These systems have a layered structure, and they are characterized by the formula MX_2; M represents a transition metal ion (M = Ti, Zr, Hf, V, Nb, Ta, Mo, W, and Re), while X denotes a chalcogen atom (X = S, Se, Te) [18,37]. Each layer is constituted by a hexagonal transition-metal sheet sandwiched between two analogous chalcogen layers, which are coupled to each other via weak van der Waals (vdW) forces. Within the layers, they form-bonded, two-dimensional $X-X$ layers, while M has either trigonal prismatic or octahedral coordination with X [22]. In some of these systems, the induction of superconductivity can be achieved through the intercalation of a variety of elements into the van der Waals gaps [8–10], the application of pressure [11,12], or the application of gate voltages [13]. Importantly, the electronic phase diagram, as a function of external perturbations like chemical doping or pressure, is analogous to those of high-T_C cuprates, as well to some iron-based superconductors, suggesting the role of Mottness in the emergence of superconductivity at a low T in these vdW systems. However, the physical origin for stabilizing the pseudogapped state [21,22,31–33], which is the precursor to the CDW–Mott [17] phase, has not been well understood, and this is one of our focuses here.

Similar to cuprates and some Fe-based superconductors, the 2H-polymorph $TaSe_2$ shows a strange metal, T-linear resistivity [22] in the normal state at a high T, which enters into an incommensurate CDW phase at a T close to 122 K, followed by a transition to a commensurate CDW phase near to 90 K [49,50]. Angle-resolved photoemission spectroscopy (ARPES) and optical spectroscopy data suggest the presence of a low-energy pseudogap for T above 122 K, similar to that observed in high-T_C cuprates and Fe-based superconductors. Notably, from room-T down to the CDW-phase transition, the resistivity of Pd-intercalated 2H-$TaSe_2$ [22] and 2H-$TaSe_{1-x}S_x$ [23] systems decreases nearly linearly with T [22], a characteristic akin to the strange-metal phase in which the resistivity varies linearly over a broad T range [51]. Upon entering the CDW phase, the resistivity shows a Fermi liquid (FL)-like T^2 dependence at a low T [22], implying the importance of self-energy corrections [20] in the CDW phase. Therefore, clarifying the role of electron correlations [17,46,52] in the delicate balance between the CDW and non-CDW phases is necessary. Motivated by this and the fact that 2H-$TaSe_2$ is considered to be a promising material for nano-electronic devices, as well as a material for flexible, two-dimensional (2D) optoelectronic applications [53], in this work, we derive the electronic properties of a $\mathcal{TB}$ [39] extended Hubbard model similar to that proposed for bilayer cuprate superconductors [54], showing the role of dynamical correlations in the non-CDW and CDW ordered states of 2H-$TaSe_2$. Our results are relevant to understanding the electronic structure modification that could result in the creation of BCS-like s-wave [33] superconductivity at a low T, as well as the emergence of CDW–Mott localization [22] in the vicinity of a correlation-induced quantum phase transition [2].

2. Theory and Results

Based on Ref. [39], the two-band ($\mathcal{TB}$) tight-binding model considered in this work reads as

$$H_{TB}(\mathbf{k}) = f(t_0, t_1, t_2; \mathbf{k})\sigma_0 + f(\tilde{t}_0, \tilde{t}_1, \tilde{t}_2; \mathbf{k})\sigma_x \,, \tag{1}$$

$$f(\alpha,\beta,\gamma;\mathbf{k}) = \alpha + 2\beta\left[cosk_xa + 2cos\frac{k_xa}{2}cos\frac{\sqrt{3}k_xa}{2}\right] + 2\gamma\left[cos\sqrt{3}k_ya + 2cos\frac{3k_xa}{2}cos\frac{\sqrt{3}k_ya}{2}\right],$$

where σ_0 is a (2×2) identity matrix, σ_x is the x Pauli matrix, $a = 3.43$ Å is the lattice constant of $2H$-$TaSe_2$, $t_0 = 0.113$ eV is the Ta on-site energy, $\tilde{t}_0 = 0.184$ eV is the direct interlayer coupling, and $t_1 = 0.073$ eV ($\tilde{t}_1 = 0.029$ eV) and $t_2 = 0.142$ eV ($\tilde{t}_2 = 0.038$ eV) are the nearest- and next-nearest intralayer (interlayer) couplings. In Ref. [39], the one-particle parameters were fixed using a hybrid approach that fits the tight-binding (TB) model to the ARPES data below the Fermi level (E_F) and density functional theory (DFT) calculations above it. It is noteworthy that, while the $f\times\sigma_0$ contribution to $H_{TB}(\mathbf{k})$ (in Equation (2)) stands for the diagonalized band dispersion, $\varepsilon_a(\mathbf{k})$, of the $a\,(\neq b) = 1,2$ bands, the $f\times\sigma_x$ term in $H_{TB}(\mathbf{k})$ corresponds to a non-local, $\mathbf{k}$-dependent hybridization [55–57] (here denoted as $\mathcal{V}(\mathbf{k})$) between the two a-bands of $2H$-$TaSe_2$ crossing E_F, as reported in Ref. [39]. Finally, we shall mention here that, according to the ARPES data of Ref. [39], the dispersions $\varepsilon_a(\mathbf{k})$ are split by an energy Δ of the order of 0.15 eV; thus, in our study, we set $\varepsilon_1(\mathbf{k}) = \Delta + \varepsilon_2(\mathbf{k})$. These are the relevant one-particle inputs to $\mathcal{TB}$+DMFT [54], which generates a strongly renormalized $\mathcal{TB}$ electronic state due to correlation and CDW effects. The local (U,U') and non-local (V) interactions of $2H$-$TaSe_2$ are contained in $H_{int} = U\sum_{i,a} n_{i,a,\uparrow}n_{i,a,\downarrow} + U'\sum_{i,a\neq b} n_{i,a}n_{i,b} + V\sum_{i\neq j} n_in_j$. Here, the indices i run over the lattice sites in the $a,b = 1,2$ bands. U and U' are the on-site intra- and inter-band Coulomb interactions and V is the nearest-neighbor Coulomb repulsion, all responsible for the many-particle electronic structure reconstruction in the extended $(V\neq 0)$ $\mathcal{TB}$ Hubbard model considered here for $2H$-$TaSe_2$: without a loss of generality, here, we set $U' = V = 0.8U$. Finally, as in earlier works [54,58,59], we decouple the intersite Coulomb interaction term of H_{int} in the Hartree approximation, which is exactly under the large D limit [5].

Inspired by earlier theory studies on bilayer cuprates [55,60,61], in this work, we consider an extended $\mathcal{TB}$ Hubbard model [54] for $2H$-$TaSe_2$ using hopping integrals introduced in Ref. [39] for the parent compound, as described above. We evaluate the retarded, one-particle Green's functions

$$G_{a,\sigma}(\omega,\mathbf{k}) = \left[\xi_{a,\sigma}(\omega) - \varepsilon_a(\mathbf{k}) - \frac{\mathcal{V}^2(\mathbf{k})}{\xi_{b,\sigma}(\omega) - \varepsilon_b(\mathbf{k})}\right]^{-1}, \quad (2)$$

where $\xi_{a,\sigma}(\omega) \equiv \omega + i\eta - \Sigma_{a,\sigma}(\omega + i\eta)$ [62], of the hybrid $\mathcal{TB}$ system at zero T and real frequencies using the $\mathcal{TB}$ [62] iterated perturbation theory as an impurity solver for DMFT. The detailed formulation of this algebraic DMFT solver for correlated electron systems has been introduced in the context of real materials with different charge, orbital, and spin degrees of freedom (see Refs. [63,64]). It has also been used to study the evolution of the one-particle spectra of the periodic Anderson model with the incorporation of inter-band Coulomb correlations [62]. Therefore, we do not repeat the equations here. It should be noted, however, that this interpolative *ansatz* is based on second-order perturbation theory, which takes into account all dynamical scattering processes arising from intra- and inter-band Coulomb interactions in a self-consistent manner. Furthermore, for the sake of clarity, it should be noted that, in the $\mathcal{TB}$ Hubbard model, the one-particle Green's functions of each band are coupled via the inter-band (inter-orbital in the multi-orbital case) Coulomb interaction U', as well as the k-dependent interband hybridization $\mathcal{V}(\mathbf{k})$ [55–57]. In general, our formalism can be regarded as an extension of the periodic Anderson model [5], in which the two channels are dispersive and subject to on-site electron–electron interactions, which are proximitized [65] by k-dependent interband hopping integrals [39]. As demonstrated below, the integration of realistic $\mathcal{TB}$ [39] inputs with multi-particle, many-body effects [5] provides a comprehensive account of the electronic properties of $2H$-$TaSe_2$ in both the normal and CDW states.

Let us now discuss our $\mathcal{TB}$ and $\mathcal{TB}$+DMFT results. We begin by considering the many-body Hamiltonian $H = H_{TB}(\mathbf{k}) + H_{nt}$ within the normal, non-CDW ordered state. In this regime, the two non-equivalent CDW sites A, B of the bipartite (2×2) superlattice [39] considered here will have the same electronic structures and the total on-site band fillings $n = n_A = n_B$. In Figure 1, we show the TB-based electronic state at $U = 0.0$ eV. Several features are noteworthy in this limit. Due to finite band splitting Δ [39], the unperturbed density of states (DOS) shows different lineshapes, with band two being more populated as compared to the higher-energy band, as shown in the lower and upper panels of Figure 1, respectively. From the band-resolved DOS up to the Fermi level ($E_F = \omega = 0.0$), we obtain $n_{2,\sigma} = 0.56$ and $n_{1,\sigma} = 0.44$, which would correspond to half-filled bands at $\Delta = 0.0$, i.e., one electron per band. Also notably, in the bare $\mathcal{TB}$ DOS is the particle-hole asymmetry characteristic TB models with sizable nearest and next-nearest neighbor hopping integrals [54], an aspect consistent with extant band structure calculations for $2H$-$TaSe_2$ [14]. Also interesting in the bare DOS of Figure 1 is the van Hove-like peak at 0.52 eV, binding energy in $\rho_{2,\sigma}(\omega)[= -\frac{1}{\pi} Im \sum_{\mathbf{k}} G_{2,\sigma}(\omega, \mathbf{k})]$, and the valence band edge, which almost coincides with that reported in Ref. [14], providing support for the TB model proposed in Ref. [39]. It is also noteworthy that the local spectral functions $\rho_{a,\sigma}(\omega)$ undergo changes with an increasing on-site Coulomb interaction, U, in the non-CDW limit, as illustrated in Figure 1. As can be observed in the main panel of Figure 1, the results presented correctly reproduce the expected behavior for the correlated spectral functions within the DMFT approximation. Of particular interest are the emergence of the lower (LHB) and upper (UHB) Hubbard bands at high energies and the Kondo–quasiparticle resonances [5] near E_F, which narrow with an increasing U. Furthermore, as a result of particle-hole asymmetry and the interplay between sizable U, U', and V, the pinning of the correlated spectral function to its bare value at E_F [5] obtained for the one-band Hubbard model is no longer valid in the extended $\mathcal{TB}$ Hubbard model of $2H$-$TaSe_2$. This occurs despite the fact that the self-energy imaginary parts show ω^2 dependence, which is characteristic of good FL metals [5], as can be seen in the right insets of Figure 1. However, in accordance with previous research [54,55,66], the non-CDW state of the extended $\mathcal{TB}$ Hubbard model exhibits a significant influence of many-body effects on the $U = 0.0$ DOS, resulting in a notable transfer of spectral weight from low to high energies and a discernible ω-dependence in the self-energy real and imaginary parts, as seen in Figure 1.

Let us now elucidate the evolution of the electronic structure of the correlated spectral function of $2H$-$TaSe_2$ by focusing on the total DOS $[\rho_{total}(\omega) = \sum_{a,\sigma} \rho_{a,\sigma}(\omega)]$. To this end, we have obtained the total DOS for two U values, as shown in Figure 2. As anticipated within the framework of the dynamical mean-field theory (DMFT) [5], the narrowing of the coherent Kondo-quasiparticle resonance is attributed to dynamical correlations, which also result in the enhancement of the Hubbard satellites due to the increased dynamical transfer of spectral weight with an increasing U. Of particular interest is the peak deep hump observed in the DFT+DMFT total DOS below E_F, as illustrated in the main panel of Figure 2. This finding aligns well with the energy-distribution curve (EDC) reported in Ref. [17], where the EDC curve of the pristine $1T$-$TaSe_2$ at the Γ point displays a comparable behavior, exhibiting a deep binding energy of approximately 1.0 eV, as illustrated in Figure 2. It is also noteworthy that the peak positions of the low-energy Kondo-quasiparticles blueshift [67,68] with an increasing U, a behavior associated with dynamical changes in the correlated spectral functions. Furthermore, the inset of Figure 2 presents a direct comparison between $\rho_{total}(\omega)$ and EDC curves [32] obtained at $T = 290$ K, which corresponds to the non-CDW ordered state of $2H$-$TaSe_2$. As can be observed, our results for a U between 2.0 and 2.5 eV provide a qualitative account of the main lineshape seen in the EDC curves of Ref. [32], particularly in terms of the energy position of the shoulder features and the depth of the EDC below 0.1 eV binding energy. This provides support for our modeling and parameter choice.

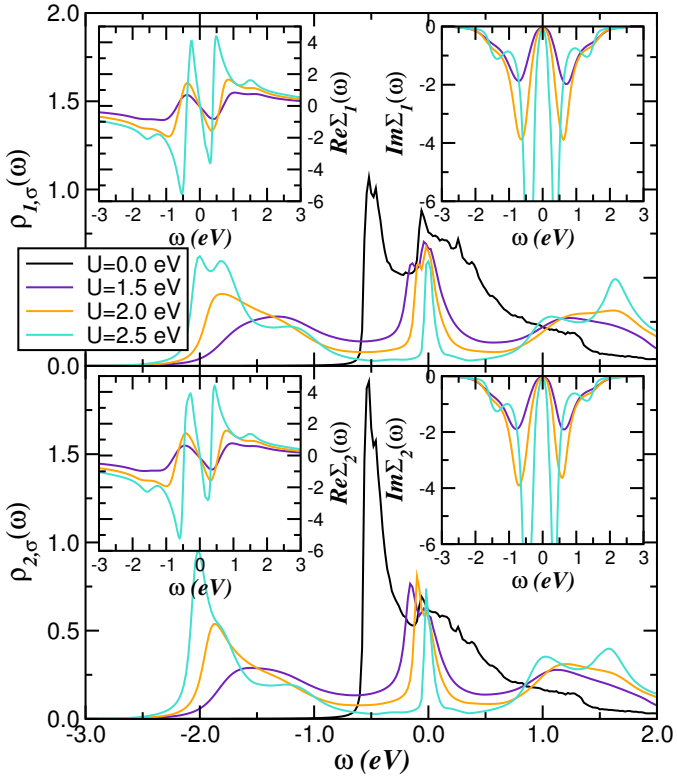

Figure 1. Local spectral functions for the extended two-band Hubbard model as a function of the on-site Coulomb repulsion U in the normal, non-CDW ordered state. Notice the particle-hole asymmetry of $U = 0.0$ eV density of states (DOS), the emergent Hubbard bands at a finite U, and the Kondo-quasiparticle resonances at low energies. The inset diplays the energy dependence of the self-energy real (left panels) and imaginary (right panels) parts for the two-band model of $2H$-$TaSe_2$, showing ω^2 dependence of $\mathrm{Im}\Sigma_{\alpha,\sigma}(\omega)$ near the Fermi energy ($E_F = \omega = 0$), a fingerprint of a Fermi liquid metal.

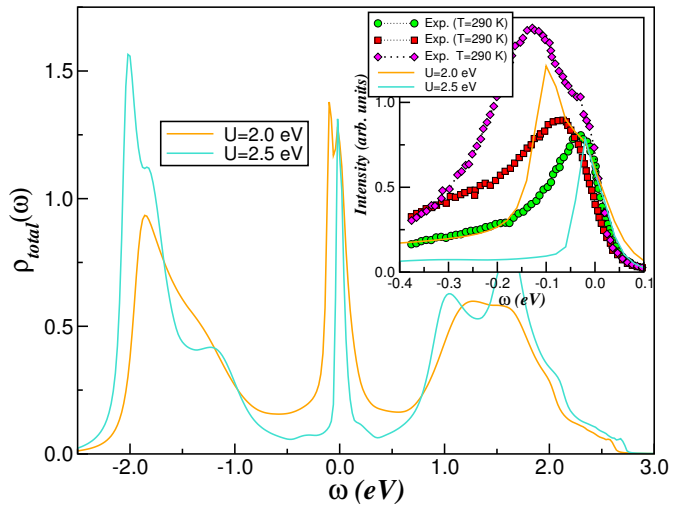

Figure 2. U-dependence of the total DOS within the non-CDW phase of $2H$-$TaSe_2$. Notice the enhancement of the Hubbard bands and the narrowing of the Kondo-quasiparticle resonance at high and low energies, respectively, induced via the dynamical transfer of spectral weight with an increasing U. The inset displays a theory-experiment comparison between the total DMFT DOS and energy-distribution curves (EDC) in the normal state along the Γ (dots), K (squares), and M (diamonds) cuts in momentum space taken from Ref. [32].

To provide additional insights into the $\mathcal{TB}$ electronic structure reconstruction 2H-$TaSe_2$, we have extended our DMFT Green's function formalism above (see Equation (2)) to incorporate the CDW degree of freedom. For the sake of simplicity, we consider here the (2×2) CDW ordered state, [39] where, similar to an antiferromagnetic spin-density wave (SDW) state [69], the four-component lattice Green's functions relevant to 2H-$TaSe_2$ can be written as

$$G_{a,\gamma,\sigma}(\omega, \mathbf{k}) = \left[\xi_{a,\sigma}(\omega) - \frac{\varepsilon_a^2(\mathbf{k})}{\xi_{\bar{\gamma},\sigma}(\omega)} - \frac{\mathcal{V}^2(\mathbf{k})}{\xi_{b,\gamma,\sigma}(\omega) - \varepsilon_b(\mathbf{k})}\right]^{-1}, \quad (3)$$

where $\gamma(\neq \bar{\gamma}) = A$ or B labels the sublattice [70] of the (2×2) CDW-induced superlattice [39].

In the main panel of Figure 3, we show the correlated spectral functions that emerge when considering a (2×2) charge ordering state [39] and $U = 2.0$ eV as a representative Coulomb interaction parameter value. To derive the CDW ordered state, we consider polarized site-resolved band fillings as the starting point towards fully self-consistent DMFT calculations, where the site B site is set to be more populated with 1.4 electrons per spin, as compared to the A site, where $n_A = 0.6$. As seen, the correlated spectral functions display site differentiation as compared to the non-CDW state where the spectral functions of sites A and B coincide. In spite of the small changes between the correlated A and B DOS in the CDW ordered state as a result of strong dynamical, particle-hole scattering processes induced via U and U', an energy gap opening associated with the occurrence of CDW [71–74] spans near E_F, resulting in the splitting of the Kondo–quasiparticle resonance into two narrow peaks for all spectral functions. Notably, a similar effect also takes place at high energies where the Hubbard bands also split into two branches. Also remarkable in Figure 3 is the stability of the self-energy real and imaginary parts against CDW, suggesting that the CDW state emerges as a result of one-particle nesting [17,71,72] due to the bipartite lattice structure of the (2×2) CDW order.

In this study, we further examine the impact of additional electron–electron interaction effects induced via dynamical many-particle correlation effects on the pseudogapped [21,22,31–33] state of the $\mathcal{TB}$ system. In contrast to the approach taken in Refs. [17,47], where different U values were considered for transition-metal dichalcogenide systems, Figure 4 presents the results obtained for U/W from 0.8 up to 1.07. Given that U' scatters electrons with opposite and equal spins, which significantly enhances electron–electron correlation effects, in Figure 4, we commence by presenting our results for the total DOS, $\rho_{total}(\omega) = \frac{1}{2}\sum_{a,\gamma,\sigma}\rho_{a,\gamma,\sigma}(\omega)$, for $U = 2.25$ eV. As can be observed, while the splitting of the LHB is robust against the combined effect of intra- and inter-band Coulomb repulsion, a reverse trend emerges at low energies with the concomitant suppression of the CDW bandgap splitting. Moreover, upon increasing U, the spectral weight transfer from quasiparticle excitations to incoherent Hubbard bands is evident in the correlated spectral function of the CDW $\mathcal{TB}$ model of 2H-$TaSe_2$. It is noteworthy that the pseudogapped state obtained for $U = 2.5$ eV diminishes, resulting in metallicity at low energies in proximity to E_F, as evidenced by our findings for $U = 2.75$ eV. Finally, to illustrate the role played by local dynamical correlations, we present in the inset of Fig. reffig4 a comparison between the DFT+DMFT total spectral function displayed in the main panel of Figure 4 and EDC data taken from Refs. [20,32]. This comparison demonstrates good qualitative agreement between the two sets of data. In particular, the shoulder features near E_F and the ω-dependence of the correlated spectra at slightly higher binding energies are accurately reproduced using the DMFT approximation for the $\mathcal{TB}$ model of 2H-$TaSe_2$.

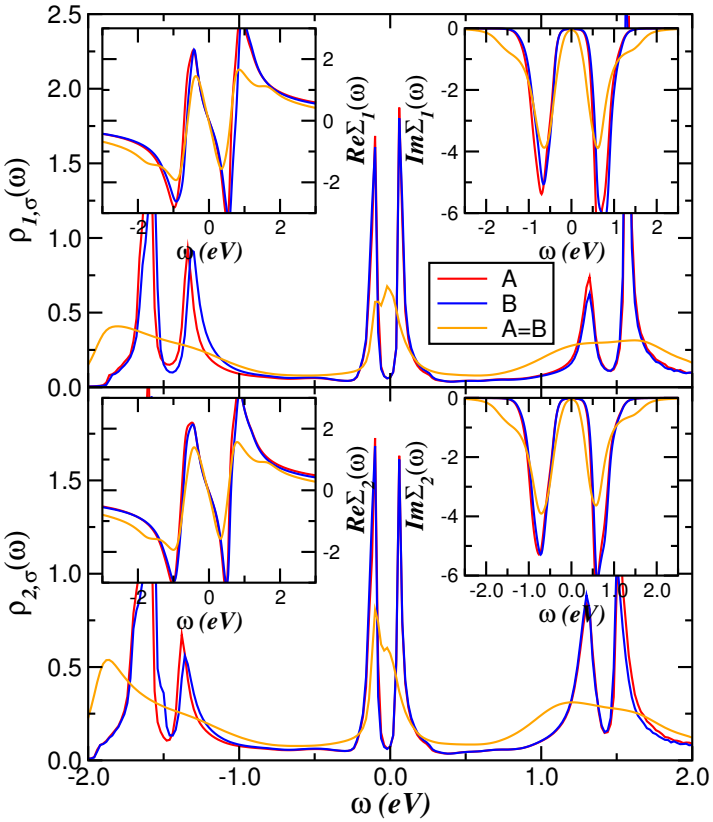

Figure 3. Comparison between site-resolved (A,B) CDW and non-CDW (A = B) DOS of $2H$-$TaSe_2$, showing the electronic reconstruction induced via the (2×2) CDW order. Particularly interesting features seem to be the CDW gap that emerges at E_F, which splits the Kondo–quasiparticle resonances into two branches. Also noteworthy are the CDW-like gaps in the Hubbard bands and the small differences in the self-energy real and imaginary parts of the insets.

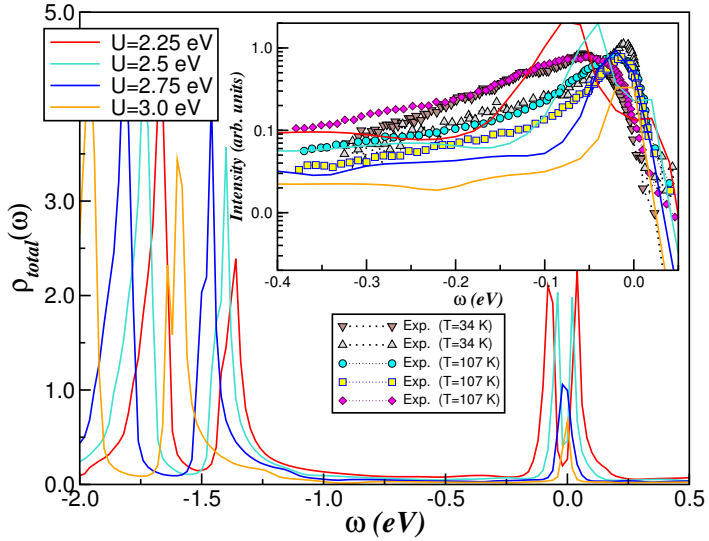

Figure 4. Evolution of the total DMFT DOS with an increasing U in the (2) CDW ordered state of $2H$-$TaSe_2$. Notice the narrowing of the electronic excitations, as well as the CDW gap, inducing a pseudogap and metallicity with an increasing U. The inset displays a theory-experiment comparison between the DMTT results and EDC data taken at 34 K [20] and 107 K: [32] The EDC data were obtained along the Γ (squares, circles, and upward triangles) and K (diamonds and downward triangles) cuts in momentum space.

Ultimately, to provide new fundamental insights into the correlated phenomenon that may emerge in strained 2H-$TaSe_2$ crystals, where $U/W \gg 1$ [2], in Figure 5, we demonstrate the ω dependence of the correlated spectra as we approach the CDW–Mott localized state [17]. Figure 5 illustrates the occurrence of gradual alterations in the total spectral functions, which suggests the existence of a second-order metal-to-insulator transition from a CDW metal to a CDW–Mott localized state. These responses are characteristic of strongly correlated systems in which the changes to the spectral functions are linked to collective electronic (charge and spin) fluctuations in the reconstructed spectral function [75]. As observed for $U = 3.5$ eV, which is in close proximity to the critical value for the continuous CDW–Mott transition, the narrow low-energy peak that was present at $U = 3.25$ eV has been almost entirely suppressed, and only the Hubbard bands are clearly discernible at high energies above and below E_F. A comparable quantum-phase transition, with the coexistence of Mott localized and metallic electronic states, has been documented in the context of the three-orbital problem of ruthenate oxides [76] and in a theoretical investigation of the $T = 0$ phase transition in two dimensions, from a Fermi liquid metal to a paramagnetic Mott insulator with a spinon Fermi surface [77]. Furthermore, the demonstration of a continuous Mott transition in $MoTe_2/WSe_2$ Moiré superlattices is also relevant in this context. This transition is induced by varying an out-of-plane electric field, which modifies the Moiré potential depth and, thus, the U/W ratio [78], and it is observed to occur as a result of the metal–insulator transition.

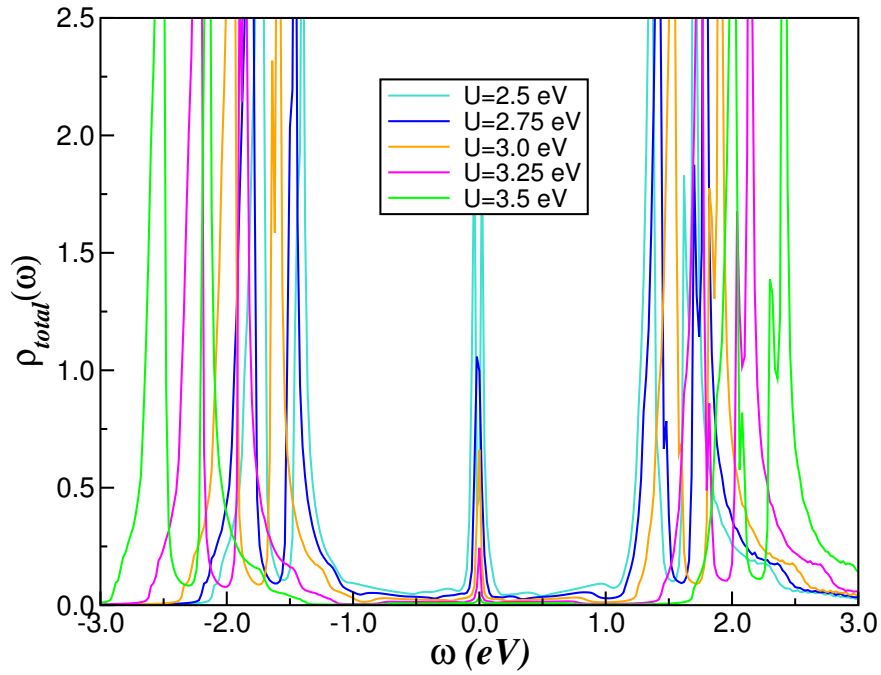

Figure 5. Illustration of the continuous metal-insulator transition induced via strong electron–electron interactions in the CDW phase of 2H-$TaSe_2$. Notice the suppression of the nearly vanished metallic total DOS for $U = 3.25$ eV to a CDW–Mott localized state at $U = 3.5$ eV.

3. Conclusions

In conclusion, this study has investigated the electronic structure reconstruction of an extended two-band Hubbard model, which is applicable to 2H-$TaSe_2$. In accordance with earlier studies, this study found that intra- and inter-band many-body effects strongly renormalize electronic structure of 2H-TaSe2 within the normal and CDW ordered states. Due to sizable dynamical two-band correlations, we demonstrated the emergence of pseudogapped electronic state consistent with experimental observations [20,32]. Moreover, in the high correlation-to-bandwidth (U/W) limit, we predict a gap-closing [79] scenario where a continuous metal–insulator transition from a CDW-gapped insulating state [73,74]

followed by a CDW–Mott [17] insulating state is demonstrated. Taken together, the results in this work constitute a step forward in understanding the manifestation of band-selective pseudogaped and CDW–Mott phases that might, respectively, be the precursors to superconductivity in S-doped 2H-$TaSe_2$ [23] and to the dimensionality-driven insulator–metal transition reported for 1T-$TaSe_2$ [80].

Funding: This research received no external funding.

Data Availability Statement: Data are available upon request to the author.

Acknowledgments: Acknowledgment is extended to CNPq and CAPES, as well as to Laurin Craco for making valuable suggestions on improving the quality of the presentation based on DeepL Write.

Conflicts of Interest: The author declare no conflicts of interest.

References

1. Mott, N.F. Metal-insulator transition. *Rev. Mod. Phys.* **1968**, *40*, 677. [CrossRef]
2. Imada, M.; Fujimori, A.; Tokura, Y. Metal-insulator transitions. *Rev. Mod. Phys.* **1998**, *70*, 1039. [CrossRef]
3. Laad, M.S.; Craco, L. Mott transition: A brief review. *Adv. Quantum Tecnol.* **2024**, 2200186. [CrossRef]
4. Bao, C.; Zhong, H.; Wang, F.; Lin, T.; Zhang, H.; Sun, Z.; Duan, W.; Zhou, S. Distinguishing and controlling Mottness in 1T-TaS_2 by ultrafast light. *Phys. Rev. B* **2023**, *107*, L121103. [CrossRef]
5. Georges, A.; Kotliar, G.; Krauth, W.; Rozenberg, M.J. Dynamical mean-field theory of strongly correlated fermion systems and the limit of infinite dimensions. *Rev. Mod. Phys.* **1996**, *68*, 13. [CrossRef]
6. Damascelli, A.; Hussain, Z.; Shen, Z.-X. Angle-resolved photoemission studies of the cuprate superconductors. *Rev. Mod. Phys.* **2003**, *75*, 473. [CrossRef]
7. Lee, P.A.; Nagaosa, N.; Wen, X.-G. Doping a Mott insulator: Physics of high-temperature superconductivity. *Rev. Mod. Phys.* **2006**, *78*, 17. [CrossRef]
8. Gamble, F.R.; Osiecki, J.H.; Cais, M.; Pisharody, R.; DiSalvo, F.J.; Geballe, T.H. Intercalation complexes of Lewis bases and layered sulfides: A large class of new superconductors. *Science* **1971**, *174*, 493. [CrossRef]
9. Morosan, E.; Zandbergen, H.W.; Dennis, B.S.; Bos, J.W.G.; Onose, Y.; Klimczuk, T.; Ramirez, A.P.; Ong, N.P.; Cava, R.J. Superconductivity in Cu_xTiSe_2. *Nature Phys.* **2006**, *2*, 544. [CrossRef]
10. Wagner, K.E.; Morosan, E.; Hor, Y.S.; Tao, J.; Zhu, Y.; Sanders, T.; McQueen, T.M.; Zandbergen, H.W.; Williams, A.J.; West, D.V.; et al. Tuning the charge density wave and superconductivity in Cu_xTaS_2. *Phys. Rev. B* **2008**, *78*, 104520. [CrossRef]
11. Kusmartseva, A.F.; Sipos, B.; Berger, H.; Forró, L.; Tutis, E. Pressure induced superconductivity in pristine 1T-$TiSe_2$. *Phys. Rev. Lett.* **2009**, *103*, 236401. [CrossRef]
12. Sipos, B.; Kusmartseva, A.F.; Akrap, A.; Berger, H.; Forró, L.; Tutiš, E. From Mott state to superconductivity in 1T-TaS_2. *Nat. Mater.* **2008**, *7*, 960. [CrossRef]
13. Yu, Y.; Yang, F.; Lu, X.F.; Yan, Y.J.; Cho, Y.-H.; Ma, L.; Niu, X.; Kim, S.; Son, Y.-W.; Feng, D.; et al. Gate-tunable phase transitions in thin flakes of 1T-TaS_2. *Nat. Nanotech.* **2015**, *10*, 270. [CrossRef]
14. Smith, N.V.; Kevan, S.D.; DiSalvo, F.J. Band structures of the layer compounds 1T-TaS_2 and 2H-$TaSe_2$ in the presence of commensurate charge-density waves. *J. Phys. C* **1985**, *18*, 3175. [CrossRef]
15. Kim, J.-J.; Yamaguchi, W.; Hasegawa, T.; Kitazawa, K. Observation of Mott localization gap using low temperature scanning tunneling spectroscopy in commensurate 1T-TaS_2. *Phys. Rev. Lett.* **1994**, *73*, 2103. [CrossRef]
16. Perfetti, L.; Gloor, T.A.; Mila, F.; Berger, H.; Grioni, M. Unexpected periodicity in the quasi-two-dimensional Mott insulator 1T-TaS_2 revealed by angle-resolved photoemission. *Phys. Rev. B* **2005**, *71*, 153101. [CrossRef]
17. Nakata, Y.; Sugawara, K.; Chainani, A.; Oka, H.; Bao, C.; Zhou, S.; Chuang, P.-Y.; Cheng, C.-M.; Kawakami, T.; Saruta, Y.; et al. Robust charge-density wave strengthened by electron correlations in monolayer 1T-$TaSe_2$ and 1T-$NbSe_2$. *Nat. Commun.* **2021**, *12*, 5873. [CrossRef]
18. Wilson, J.A.; Di Salvo, F.; Mahajan, S. Charge-density waves and superlattices in the metallic layered transition metal dichalcogenides. *Adv. Phys.* **1975**, *24*, 117. [CrossRef]
19. Scruby, C.; Williams, P.; Parry, G. The role of charge density waves in structural transformations of 1T-TaS_2. *Philos. Mag.* **1975**, *31*, 255. [CrossRef]
20. Valla, T.; Fedorov, A.V.; Johnson, P.D.; Xue, J.; Smith, K.E.; DiSalvo, F.J. Charge-density-wave-induced modifications to the quasiparticle self-energy in 2H-$TaSe_2$. *Phys. Rev. Lett.* **2000**, *85*, 4759. [CrossRef]
21. Baek, S.-H.; Sur, Y.; Kim, K.K.; Vojta, M.; Büchner, B. Interplay of charge density waves, disorder, and superconductivity in 2H-$TaSe_2$ elucidated by NMR. *New J. Phys.* **2022**, *24*, 043008. [CrossRef]
22. Bhoi, D.; Khim, S.; Nam, W.; Lee, B.S.; Kim, C.; Jeon, B.-G.; Min, B.H.; Park, S.; Kim, K.H. Interplay of charge density wave and multiband superconductivity in 2H-Pd_xTaSe_2. *Sci. Rep.* **2016**, *6*, 24068. [CrossRef]
23. Xu, S.; Liu, Z.; Yang, P.; Chen, K.; Sun, J.; Dai, J.; Yin, Y.; Hong, F.; Yu, X.; Xue, M.; et al. Superconducting phase diagrams of S-doped 2H-$TaSe_2$ under hydrostatic pressure. *Phys. Rev. B* **2020**, *102*, 184511. [CrossRef]

24. Zhong, A.; Shen, X.; Kogar, A.; Ye, L.; Marks, C.; Chowdhury, D.; Rohwer, T.; Freelon, B.; Weathersby, S.; Li, R.; et al. Ultrafast manipulation of mirror domain walls in a charge density wave. *Sci. Adv.* **2018**, *4*, eaau5501. [CrossRef]
25. Petkov, V.; Peralta, J.E.; Aoun, B. Ren, Y. Atomic structure and Mott nature of the insulating charge density wave phase of 1*T*-TaS_2. *J. Phys. Condens. Matter.* **2022**, *34*, 345401. [CrossRef]
26. Zwick, F.; Berger, H.; Vobornik, I.; Margaritondo, G.; Forra, F.; Beeli, C.; Onellion, M.;Panaccione, G.; Taleb-Ibrahimi, A.; Grioni, M. Spectral Consequences of Broken Phase Coherence in 1*T*−TaS_2. *Phys. Rev. Lett.* **1998**, *81*, 1058. [CrossRef]
27. Law, K.T.; Lee, P.A. 1*T*-TaS_2 as a quantum spin liquid. *Proc. Natl. Acad. Sci. USA* **2017**, *114*, 6996. [CrossRef]
28. Tosatti, E.; Fazekas, P. On the nature of the low-temperature phase of 1*T*-TaS_2. *J. Phys. Colloq.* **1976**, *37*, 165. [CrossRef]
29. Tosatti, E.; Fazekas, P. Electrical, structural and magnetic properties of pure and doped 1*T*-TaS_2. *Phil. Mag. B* **1979**, *39*, 4.
30. Crippa, L.; Bae, H.; Wunderlich, P.; Mazin, I.I.; Yan, B.; Sangiovanni, G.; Wehling, T.; Valenti, R. Heavy fermions vs doped Mott physics in heterogeneous Ta-dichalcogenide bilayers. *Nat. Commun.* **2024**, *15*, 1357. [CrossRef]
31. Zhao, J.; Wijayaratne, K.; Butler, A.; Yang, J.; Malliakas, C.D.; Chung, D.Y.; Louca, D.; Kanatzidis, M.G.; van Wezel, J.; Chatterjee, U. Orbital selectivity causing anisotropy and particle-hole asymmetry in the charge density wave gap of 2*H*-TaS_2. *Phys. Rev. B* **2017**, *96*, 125103. [CrossRef]
32. Borisenko, S.V.; Kordyuk, A.A.; Yaresko, A.N.; Zabolotnyy, V.B.; Inosov, D.S.; Schuster, R.; Büchner, B.; Weber, R.; Follath, R.; Patthey, L.; et al. Pseudogap and charge density waves in two dimensions. *Phys. Rev. Lett.* **2008**, *100*, 196402. [CrossRef]
33. Galvis, J.A.; Rodière, P.; Guillamon, I.; Osorio, M.R.; Rodrigo, J.G.; Cario, L.; Navarro-Moratalla, E.; Coronado, E.; Vieira, S.; Suderow, H. Scanning tunneling measurements of layers of superconducting 2*H*-$TaSe_2$: Evidence for a zero-bias anomaly in single layers. *Phys. Rev. B* **2013**, *87*, 094502. [CrossRef]
34. Klemm, R.A. Striking similarities between the pseudogap phenomena in cuprates and in layered organic and dichalcogenide superconductors. *Phys. C Supercond.* **2000**, *341–348*, 839. [CrossRef]
35. Vescoli, V.; Degiorgi, L.; Berger, H.; Forró, L. Dynamics of correlated two-dimensional materials: The 2*H*-$TaSe_2$ case. *Phys. Rev. Lett.* **1998**, *81*, 453. [CrossRef]
36. Ruzicka, B.; Degiorgi, L.; Berger, H.; Gaál, R.; Forró, L. Charge dynamics of 2*H*-$TaSe_2$ along the less-conducting *c*-axis. *Phys. Rev. Lett.* **2001**, *86*, 4136. [CrossRef]
37. Rossnage, K. On the origin of charge-density waves in select layered transition-metal dichalcogenides. *J. Phys. Condens. Matter* **2011**, *23*, 213001. [CrossRef]
38. Zhang, K.; Si, C.; Lian, C.-S.; Zhou, J.; Sun, Z. Mottness collapse in monolayer 1*T*-$TaSe_2$ with persisting charge density wave order. *J. Mater. Chem. C* **2020**, *8*, 9742. [CrossRef]
39. Luckin, W.R.B.; Li, Y.; Jiang, J.; Gunasekera, S.M.; Wen, C.; Zhang, Y.; Prabhakaran, D.; Flicker, F.; Chen, Y.; Mucha-Kruczynski, M. Controlling charge density order in 2*H*-$TaSe_2$ using a van Hove singularity. *Phys. Rev. Res.* **2024**, *6*, 013088. [CrossRef]
40. Suzuki, M.-T.; Harima, H. Electronic band structures and charge density wave of $2H - MX_2$ (M =Nb,Ta, X = S,Se). *Phys. B Condens. Matter* **2005**, *359*, 1180. [CrossRef]
41. Inosov, D.S.; Evtushinsky, D.V.; Zabolotnyy, V.B.; Kordyuk, A.A.; Büchner, B.; Follath, R.; Berger, H.; Borisenko, S.V. Temperature-dependent Fermi surface of 2*H*-$TaSe_2$ driven by competing density wave order fluctuations. *Phys. Rev. B* **2009**, *79*, 125112. [CrossRef]
42. Darancet, P.; Millis, A.J.; Marianetti, C.A. Three-dimensional metallic and two-dimensional insulating behavior in octahedral tantalum dichalcogenides. *Phys. Rev. B* **2014**, *90*, 045134. [CrossRef]
43. Yu, X.-L.; Liu, D.-Y.; Quan, Y.-M.; Wu, J.; Lin, H.-Q.; Chang, K.; Zou, L.-J. Electronic correlation effects and orbital density wave in the layered compound 1*T*-TaS_2. *Phys. Rev. B* **2017**, *96*, 125138. [CrossRef]
44. Yi, S.; Zhang, Z.; Cho, J.-H. Coupling of charge, lattice, orbital and spin degrees of freedom in charge density waves in 1*T*-Tas_2. *Phys. Rev. B* **2018**, *97*, 041413. [CrossRef]
45. Chen, Y.; Ruan, W.; Wu, M.; Tang, S.; Ryu, H.; Tsai, H.-Z.; Lee, R.L.; Kahn, S.; Liou, F.; Jia, C.; et al. Strong correlations and orbital texture in single-layer 1*T*-$TaSe_2$. *Nat. Phys.* **2020**, *16*, 218. [CrossRef]
46. Chen, Y.; Ruan, W.; Cain, J.D.; Lee, R.L.; Kahn, S.; Jia, C.; Zettl, A.; Crommie, M.F. Observation of a multitude of correlated states at the surface of bulk 1*T*-$TaSe_2$ crystals. *Phys. Rev. B* **2022**, *106*, 075153. [CrossRef]
47. Ramezani, H.R.; Şaşıoğlu, E.; Hadipour, H.; Soleimani, H.R.; Friedrich, C.; Blügel, S.; Mertig, I. Nonconventional screening of Coulomb interaction in two-dimensional semiconductors and metals: A comprehensive constrained random phase approximation study of MX_2 (M = Mo, W, Nb, Ta; X = S, Se, Te). *Phys. Rev. B* **2024**, *109*, 125108. [CrossRef]
48. Hwang, J.; Ruan, W.; Chen, Y.; Tang, S.; Crommie, M.F.; Shen, Z.-X.; Mo, S.-K. Charge density waves in two-dimensional transition metal dichalcogenides. *Rep. Prog. Phys.* **2024**, *87*, 044502. [CrossRef] [PubMed]
49. Moncton, D.E.; Axe, J.D.; DiSalvo, F.J. Study of superlattice formation in 2*H*-$NbSe_2$ and 2*H*-$TaSe_2$ by neutron scattering. *Phys. Rev. Lett.* **1975**, *34*, 734. [CrossRef]
50. Moncton, D.E.; Axe, J.D.; DiSalvo, F.J. Neutron scattering study of the charge-density wave transitions in 2*H*-$TaSe_2$ and 2*H*-$NbSe_2$. *Phys. Rev. B* **1977**, *16*, 801. [CrossRef]
51. Craco, L.; Leoni, S. Strange metal and coherence-incoherence crossover in pressurized $La_3Ni_2O_7$. *Phys. Rev. B* **2024**, *109*, 165116. [CrossRef]
52. Van Loon, E.G.C.P.; Schl̈er, M.; Springer, D.; Sangiovanni, G.; Tomczak, J.M.; Wehling, T.O. Coulomb engineering of two-dimensional Mott materials. *NPJ 2D Mater. Appl.* **2023**, *7*, 47. [CrossRef]

53. Mahajan, M.; Kallatt, S.; Dandu, M.; Sharma, N.; Gupta, S.; Majumdar, K. Light emission from the layered metal 2*H*-$TaSe_2$ and its potential applications. *Commun. Phys.* **2019**, *2*, 88. [CrossRef]
54. Craco, L. Electronic properties of normal and extended Hubbard model for bilayer cuprates. *Eur. Phys. J. B* **2022**, *95*, 125. [CrossRef]
55. Liechtenstein, A.I.; Gunnarsson, O.; Andersen, O.K.; Martin, R.M. Quasiparticle bands and superconductivity in bilayer cuprates. *Phys. Rev. B* **1996**, *54*, 12505. [CrossRef]
56. Hofmann, F.; Potthoff, M. Time-dependent Mott transition in the periodic Anderson model with nonlocal hybridization. *Eur. Phys. J. B* **2016**, *89*, 178. [CrossRef]
57. Segal, D.; Millis, A.J.; Reichman, D.R. Nonequilibrium transport in quantum impurity models: Exact path integral simulations. *Phys. Chem. Chem. Phys.* **2011**, *13*, 14378. [CrossRef] [PubMed]
58. Craco, L.; Ladd, M.S.; Müller-Hartmann, E. Verwey transition in Fe_3O_4 investigated using LDA+DMFT. *Phys. Rev. B* **2006**, *74*, 064425. [CrossRef]
59. Craco, L.; Laad, M.S.; Leoni, S.; de Arruda, A.S. Kondoesque origin of resistivity anisotropy in graphite. *Phys. Rev. B* **2013**, *87*, 155109. [CrossRef]
60. Chakravarty, S.; Sudbo, A.; Anderson, P.W.; Strong, S. Interlayer tunneling and gap anisotropy in high-temperature superconductors. *Science* **1993**, *261*, 337. [CrossRef]
61. Kordyuk, A.A.; Borisenko, S.V.; Knupfer, M.; Fink, J. Measuring the gap in angle-resolved photoemission experiments on cuprates. *Phys. Rev. B* **2003**, *67*, 064504. [CrossRef]
62. Craco, L. Quantum orbital entanglement: A view from the extended periodic Anderson model. *Phys. Rev. B* **2008**, *77*, 125122. [CrossRef]
63. Laad, M.S.; Craco, L.; Müller-Hartmann, E. Orbital switching and the first-order insulator-metal transition in paramagnetic V_2O_3. *Phys. Rev. Lett.* **2003**, *91*, 156402. [CrossRef] [PubMed]
64. Craco, L.; Laad, M.S.; Müller-Hartmann, E. Orbital Kondo effect in CrO_2: A combined local-spin-density-approximation dynamical-mean-field-theory study. *Phys. Rev. Lett.* **2003**, *90*, 237203. [CrossRef] [PubMed]
65. Craco, L. Correlated nature of hybrid $s-$wave superconducting and Rashba lattices. *Phys. Rev. B* **2021**, *104*, 064509. [CrossRef]
66. Fulterer, A.M.; Arrigoni, E. Correlation-induced suppression of bilayer splitting in high-T_c cuprates: A variational cluster approach. *J. Supercond. Nov. Magn.* **2012**, *25*, 1769. [CrossRef]
67. Sha, T.; Li, W.; Chen, S.; Jiang, K.; Zhu, J.; Hu, Z.; Huang, Z.; Chu, J.; Kokh, K.A.; Andreev, Y.M. Effects of S-doping on the electronic transition, band gap, and optical absorption of $GaSe_{1-x}S_x$ single crystals. *J. Alloys Compd.* **2017**, *721*,164. [CrossRef]
68. Attaccalite, C.; Prete, M.S.; Palummo, M.; Pulci, O. Interlayer and intralayer excitons in AlN/WS_2 heterostructure. *Materials* **2022**, *15*, 8318. [CrossRef]
69. Craco, L. Theoretical investigation into the possibility of multiorbital magnetically ordered states in isotropically superstrained graphene. *Phys. Rev.* **2017**, *96*, 165412. [CrossRef]
70. Craco, L.; Gusmão, M.A. Tight-binding treatment of the Hubbard model in infinite dimensions. *Phys. Rev. B* **1996**, *54*, 1629. [CrossRef]
71. Sugawara, K.; Nakata, Y.; Fujii, K.; Nakayama, K.; Souma, S.; Takahashi, T.; Sato, T. Monolayer VTe_2: Incommensurate Fermi surface nesting and suppression of charge density waves. *Phys. Rev. B* **2019**, *99*, 241404. [CrossRef]
72. Wu, Q.; Wang, Z.; Guo, Y.; Yang, F.; Gao, C. Orbital-collaborative charge density waves in monolayer VTe_2. *Phys. Rev. B* **2020**, *101*, 205105. [CrossRef]
73. Van Efferen, C.; Berges, J.; Hall, J.; van Loon, E.; Kraus, S.; Schobert, A.; Wekking, T.; Huttmann, F.; Plaar, E.; Rothenbach, N.; et al. A full gap above the Fermi level: The charge density wave of monolayer VS_2. *Nat. Commun.* **2021**, *12*, 6837. [CrossRef]
74. Knispel, T.; Berges, J.; Schobert, A.; van Loon, E.G.C.P.; Jolie, W.; Wehling, T.; Michely, T.; Fischer, J. Unconventional charge-density-wave gap in monolayer NbS_2. *Nano Lett.* **2024**, *24*, 1045. [CrossRef] [PubMed]
75. Vandelli, M.; Kaufmann, J.; Harkov, V.; Lichtenstein, A.I.; Held, K.; Stepanov, E.A. Extended regime of coexisting metallic and insulating phases in a two-orbital electronic system. *Phys. Rev. Res.* **2023**, *5*, L022016. [CrossRef]
76. Song, Z.-Y.; Jiang, X.-C.; Zhang, Y.-Z. Orbitally selective breakdown of the Fermi liquid and simultaneous enhancement of metallic and insulating states in correlated multiband systems with spin-orbit coupling. *Phys. Rev. B* **2020**, *102*, 245124. [CrossRef]
77. Senthil, T. Theory of a continuous Mott transition in two dimensions. *Phys. Rev. B* **2008**, *78*, 045109. [CrossRef]
78. Li, T.; Jiang, S.; Li, L.; Zhang, Y.; Kang, K.; Zhu, J.; Watanabe, K.; Taniguchi, T.; Chowdhury, D.; Fu, L.; et al. Continuous Mott transition in semiconductor moiré superlattices. *Nature* **2021**, *597*, 350. [CrossRef]
79. Abanov, A.; Wu, Y.-M.; Wang, Y.; Chubukov, A.A. Superconductivity above a quantum critical point in a metal: Gap closing versus gap filling, Fermi arcs, and pseudogap behavior. *Phys. Rev. B* **2019**, *99*, 180506. [CrossRef]
80. Tian, N.; Huang, Z.; Jang, B.G.; Guo, S.; Yan, Y.-J.; Gao, J.; Yu, Y.; Hwang, J.; Tang, C.; Wang, M.; et al. Dimensionality-driven metal to Mott insulator transition in two-dimensional 1*T*-$TaSe_2$. *Natl. Sci. Rev.* **2024**, *1*, nwad144. [CrossRef]